Supplementary Information (SI) for Green Chemistry.

Thermodynamically Stabilized and Driven Synthesis of Multicomponent High-Entropy Alloy Catalysts for HER

Mengxin Chen, [a] Yuji Gao, [a] Shuai Wang, [a] Furong Tao, [a] Jingui Wang, [a] Liwei Niu, [a] Hao Fang, [a] Chao Wang, [b] Guangqiang Lv [a*]

[a] School of Chemistry and Chemical Engineering, Qilu University of Technology (Shandong Academy of Sciences), Jinan 250353, Shandong, China. E-mail: lvguangqiang@qlu.edu.cn;

[b] State Key Laboratory of Biobased Material and Green Papermaking, Qilu University of Technology, Jinan 250353, Shandong, China.

1. **Materials**
2. **Synthesis of catalyst**
3. **Characterization**
4. **Electrochemical measurements**
5. **Figure S1. (a,b) TEM images of HEA-5, (c) particle-size distribution histogram of HEA-5, and (d) corresponding elemental mapping images of HEA-5**
6. **Figure S2. (a,b) TEM images of HEA-6, (c) particle-size distribution histogram of HEA-6, and (d) corresponding elemental mapping images of HEA-6**
7. **Figure S3. (a,b) TEM images of HEA-7, (c) particle-size distribution histogram of HEA-7, and (d) corresponding elemental mapping images of HEA-7**
8. **Figure S4. (a,b) TEM images of HEA-8, (c) particle-size distribution histogram of HEA-8, and (d) corresponding elemental mapping images of HEA-8**
9. **Figure S5. Particle-size distribution histogram of HEA-9**
10. **Figure S6. Particle-size distribution histogram of HEA-15**
11. **Figure S7. Survey XPS spectra of HEA-5, HEA-6, HEA-7, HEA-8, and HEA-9**
12. **Figure S8. XRD patterns of HEA-5 calcined at different holding times**

13. **Figure S9. XRD patterns of HEA-5 calcined at different calcination temperatures**
14. **Figure S10. CV curves in the non-faradaic region at different scan rates**
15. **Figure S11. Post-stability structural characterization of HEA-9 after the HER durability test.**
16. **Figure S12. Post-stability XPS spectra of HEA-9 after the HER durability test**
17. **Table S1. Mixing enthalpies of binary element pairs**
18. **Table S2. Electronegativity and covalent radius of the involved metals**
19. **Table S3. Charge-transfer resistance (R_{ct}) values of different samples**

Material and methods

1. Materials

Chloroplatinic acid hexahydrate ($H_2PtCl_6 \cdot 6H_2O$, AR Pt ⩾ 37.5%), molybdenum pentachloride ($MoCl_5$, 99.5%), palladium chloride ($PdCl_2$, 99.99%), zinc chloride ($ZnCl_2$, 98%) rhodium trichloride ($RhCl_3$, 99%) and platinum on carbon catalyst (Pt, 10%) were purchased from Macklin Biochemical Co., Ltd. (Shanghai, China). Ferric chloride hexahydrate ($FeCl_3 \cdot 6H_2O$, 99%), cobalt chloride hexahydrate ($CoCl_2 \cdot 6H_2O$, 99%), aluminum trichloride (AlCl3, AR, ≥ 99.0%) and potassium hydroxide (KOH, AR) were obtained from Sinopharm Chemical Reagent Co., Ltd. (Shanghai, China). Activated carbon powder (AR ⩾ 200 mesh), nickel chloride hexahydrate ($NiCl_2 \cdot 6H_2O$, AR, 98%), gallium(III) chloride anhydrous (GaCl3, 99.99% metals basis), and zirconium chloride (ZrCl4) and manganese chloride tetrahydrate ($MnCl_2 \cdot 4H_2O$, 99.99%) were purchased from Aladdin Biochemical Technology Co., Ltd. (Shanghai, China). Copper chloride dihydrate ($CuCl_2 \cdot 2H_2O$, 99.0%) was purchased from Shanghai Zhenxin Reagent Factory (Shanghai, China). Chromium chloride hexahydrate ($CrCl_3 \cdot 6H_2O$, AR, 99%) was obtained from Tianjin Damao Chemical Reagent Factory (Tianjin, China). Indium(III) chloride tetrahydrate (InCl3 • 4H2O, 99.99% metals basis) was purchased from 3A.

Anhydrous ethanol (CH_3CH_2OH, 99.7%) was obtained from Tianjin Fuyu Fine Chemical Co., Ltd. (Tianjin, China). Nafion solution (5%) was purchased from DuPont Co. (USA).

2. Synthesis of catalyst

Taking the preparation of $Fe_1Co_1Ni_{0.5}Cu_{0.5}Pt_1Pd_{0.5}Cr_{0.5}Mo_{0.5}Mn_{0.5}$@C as an example, 200 μl of HCl was dissolved in 10 ml of deionized water in a 25 ml beaker and ultrasonicated for 5 min. Subsequently, $FeCl_3 \cdot 6H_2O$ (4.03 mg), $CoCl_2 \cdot 6H_2O$ (3.55 mg), $NiCl_2 \cdot 6H_2O$ (1.77 mg), $CuCl_2 \cdot 2H_2O$ (1.27 mg), $H_2PtCl_6 \cdot 6H_2O$ (7.72 mg), $PdCl_2$ (1.32 mg), $CrCl_3 \cdot 6H2O$ (1.99 mg), $MoCl_5$ (2.04 mg), and $MnCl_2 \cdot 4H_2O$ (1.48 mg) were added into the solution and ultrasonicated for 60 min. Activated carbon (100 mg) was then added, followed by another 60 min ultrasonication and 2 h magnetic stirring. The resulting suspension was centrifuged at 8000 rpm for 5 min, and the black precipitate was collected and washed three times with deionized water. The washed product was dried overnight at 50 ° C to obtain a dry black powder. The powder was subsequently annealed under an Ar/H_2 atmosphere at a heating rate of 5 ° C/min to 700 ° C and maintained for 6 h, after which it was naturally cooled to room temperature to yield $Fe_1Co_1Ni_{0.5}Cu_{0.5}Pt_1Pd_{0.5}Cr_{0.5}Mo_{0.5}Mn_{0.5}$@C. The synthesis of other HEA@C catalysts followed the same procedure, with only the corresponding metal salts substituted accordingly.

3. Characterization

X-ray diffraction (XRD) patterns were collected on a Bruker diffractometer (Germany) with an operating voltage of 40 kV and a current of 40 mA, using a continuous scan rate of 10 °/min. The acquired diffraction data were processed with Jade 6.5 software, and phase identification was performed by matching the characteristic peaks with standard database references. X-ray photoelectron spectroscopy (XPS) was performed on a Thermo Scientific K-Alpha spectrometer equipped with a microfocused monochromatic Al Kα source. Measurements were conducted at room temperature under ultra-high vacuum (10^{-7} mbar) with a pass energy of 30 eV to minimize charging effects. All binding energies were referenced to the C 1s peak at 284.8 eV, and spectral deconvolution was carried out using Avantage software (Thermo Scientific). The morphology and microstructure of the samples were examined using a FEI Talos F200x transmission electron microscope (TEM, USA), and elemental analysis was performed via energy-dispersive X-ray spectroscopy (EDS) on the same instrument. Lattice fringes were analyzed by Fourier transform processing with DigitalMicrograph software, while particle size distribution was determined using ImageJ software.

4. Electrochemical measurements

2 mg of the catalyst was dispersed in a mixture of 100 μL anhydrous ethanol, 100 μL deionized water, and 4 μL Nafion solution, followed by stirring for 1 h to achieve uniform dispersion. The resulting black ink was drop-cast onto a carbon paper substrate (1 cm × 1 cm) and dried in a forced-air oven at 40 °C for 4 h, yielding a catalyst electrode with an average mass loading of 2 mg/cm^2.

Electrochemical measurements were carried out on a CHI 760E workstation at room temperature. The HER activity was evaluated in 1 M KOH electrolyte using a three-electrode system consisting of the prepared electrode as the working electrode, a Pt foil as the counter electrode, and a Hg/HgO electrode as the reference electrode. Linear sweep voltammetry (LSV) was performed at a scan rate of 10 mV/s with 95% iR compensation. All potentials were calibrated to the reversible hydrogen electrode (RHE) according to the Nernst equation:

$$E(RHE) = E(Hg/HgO) + 0.059 \times pH + 0.098\,V.$$

The Tafel slope was derived from the polarization curves. Catalyst durability was assessed by chronoamperometry in alkaline solution at a current density of 10 mA/cm^2 and 100 mA/cm^2. Electrochemical impedance spectroscopy (EIS) measurements were performed in a conventional three-electrode configuration over the frequency range of 0.01-10^5 Hz, at the potential corresponding to a current density of 10 $mA \cdot cm^{-2}$. The EIS spectra were fitted using an equivalent circuit model in Zview2, which comprised solution resistance (R_s), a constant phase element (CPE), and charge-transfer resistance (R_{ct}), in order to probe the kinetic characteristics of the system. Notably, R_{ct} reflects the charge-transfer resistance associated with the Faradaic HER and serves as a critical parameter for evaluating the catalytic kinetics. Cyclic voltammetry (CV) measurements were performed within the potential range of -0.03 to -0.13 V versus RHE at scan rates of 10, 20, 30, 40, and 50 mV/s. The double-layer capacitance (C_{dl}) was calculated from the slope of $C_{dl}=\Delta J/v$, where ΔJ represents the difference between anodic and cathodic current densities, and v is the scan rate. The electrochemically active surface area (ECSA) was estimated using the empirical equation ECSA = C_{dl} / C_s.

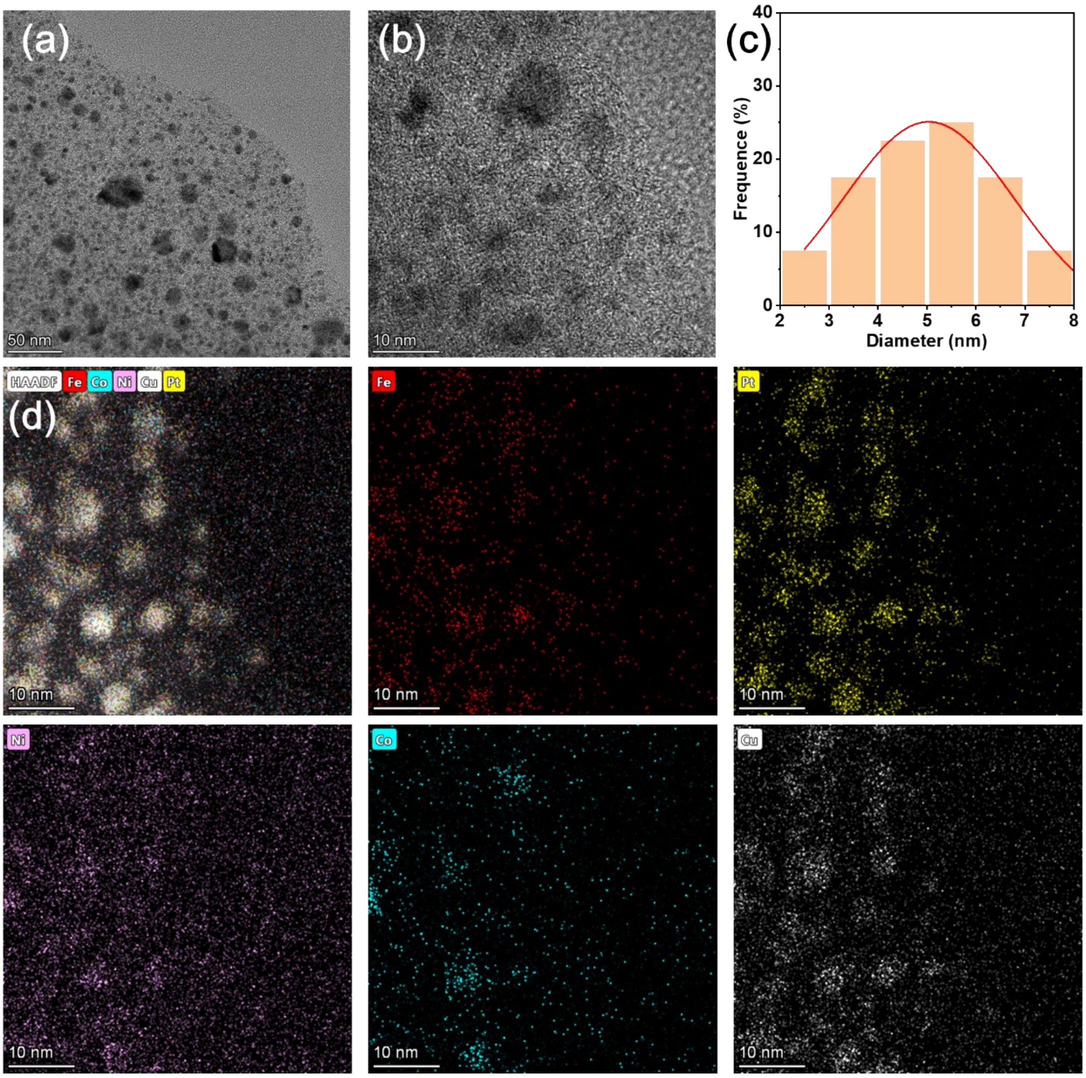

Figure S1. (a-b) TEM images of the HEA-5; (c) The particle size distribution diagram of HEA-5; (d) Mapping images of the HEA-5.

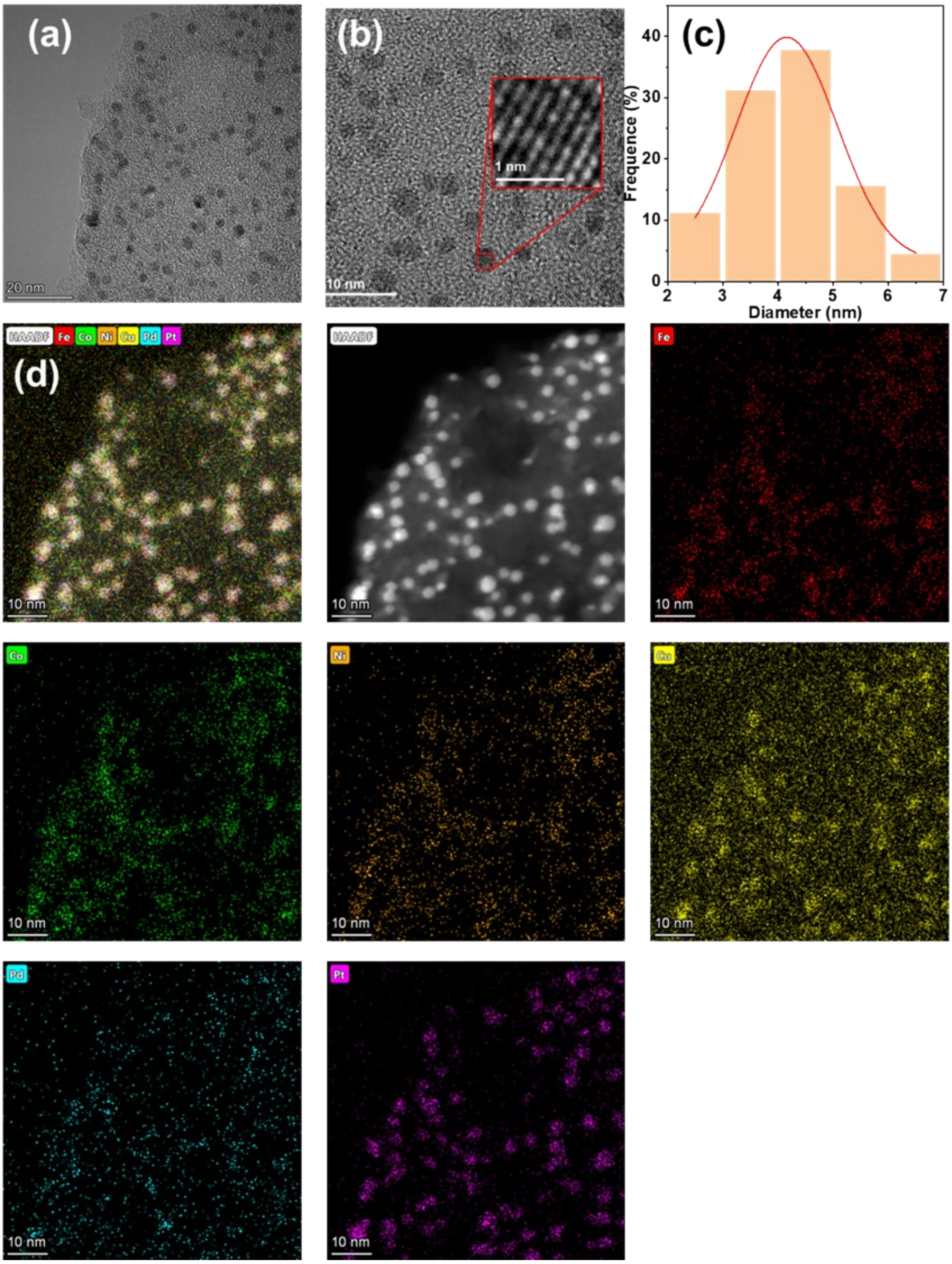

Figure S2. (a-b) TEM images of the HEA-6; (c) The particle size distribution diagram of HEA-6; (d) Mapping images of the HEA-6

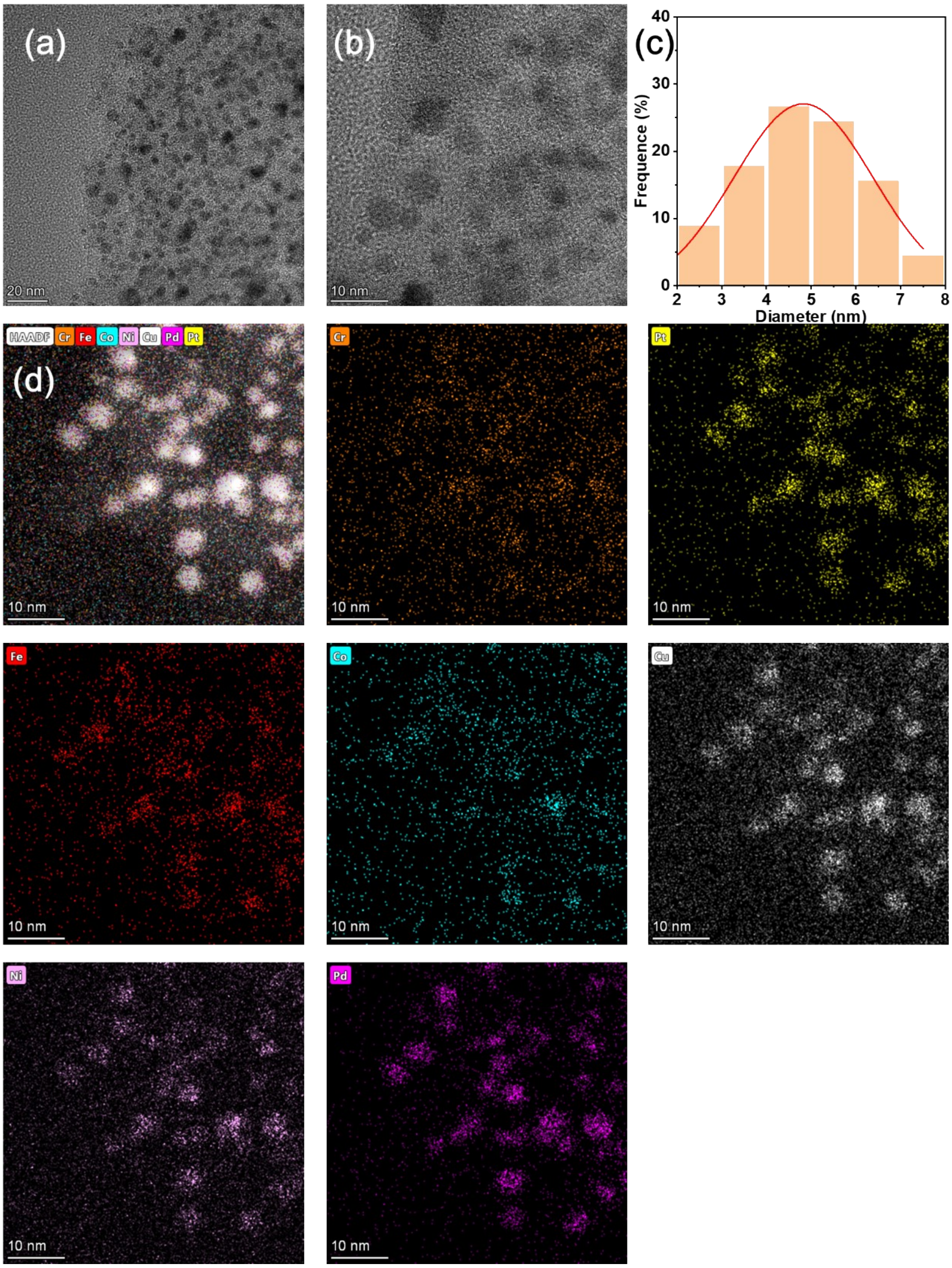

Figure S3. (a-b) TEM images of the HEA-7; (c) The particle size distribution diagram of HEA-7; (d) Mapping images of the HEA-7

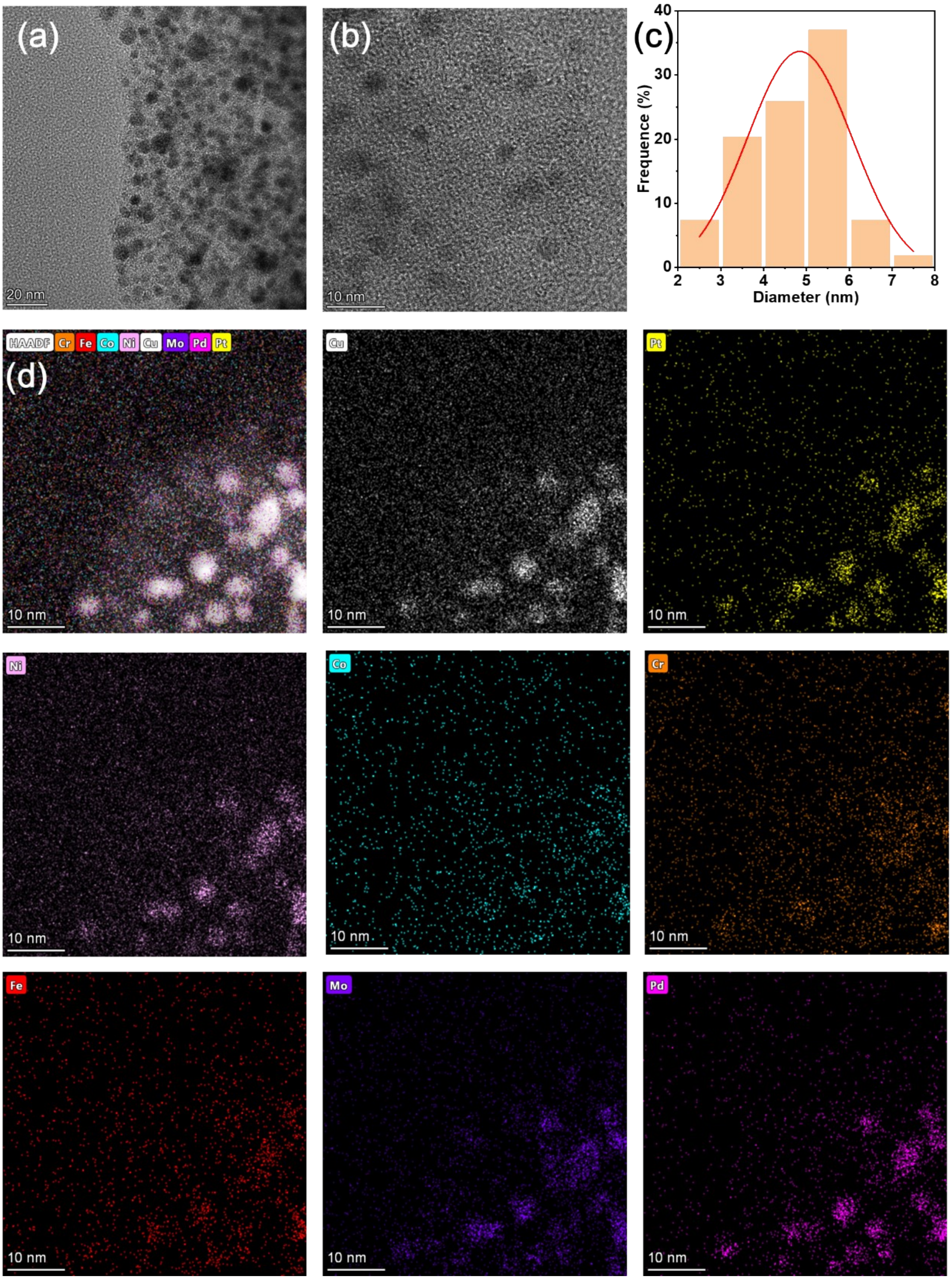

Figure S4. (a-b) TEM images of the HEA-8; (c) The particle size distribution diagram of HEA-8; (d) Mapping images of the HEA-8

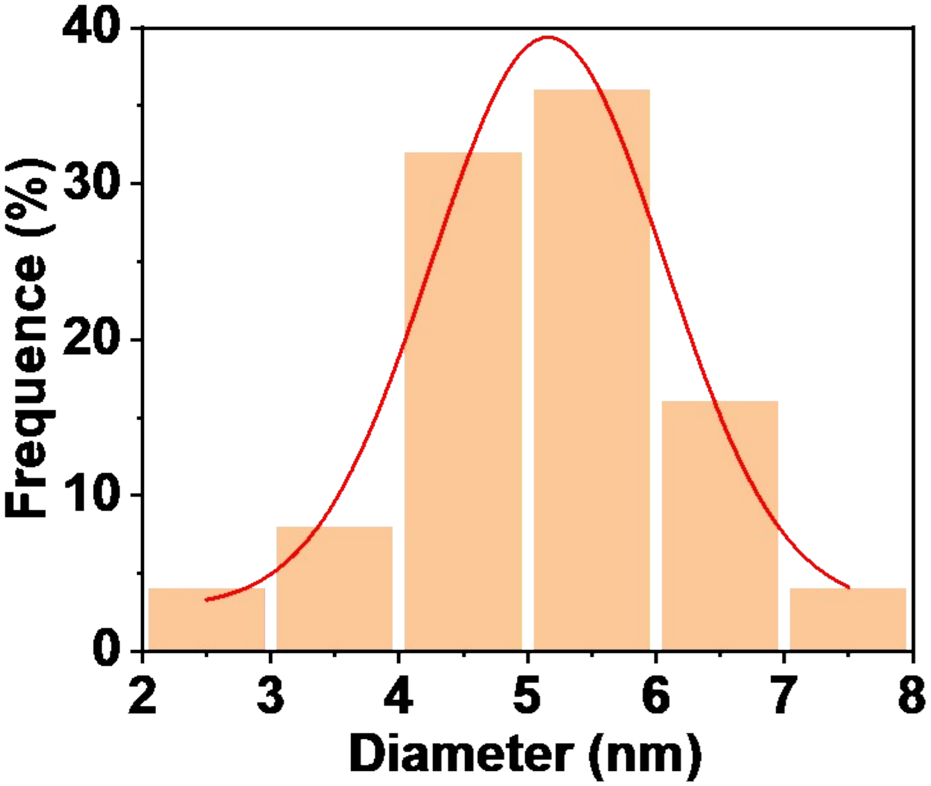

Figure S5. The particle size distribution diagram of HEA-9

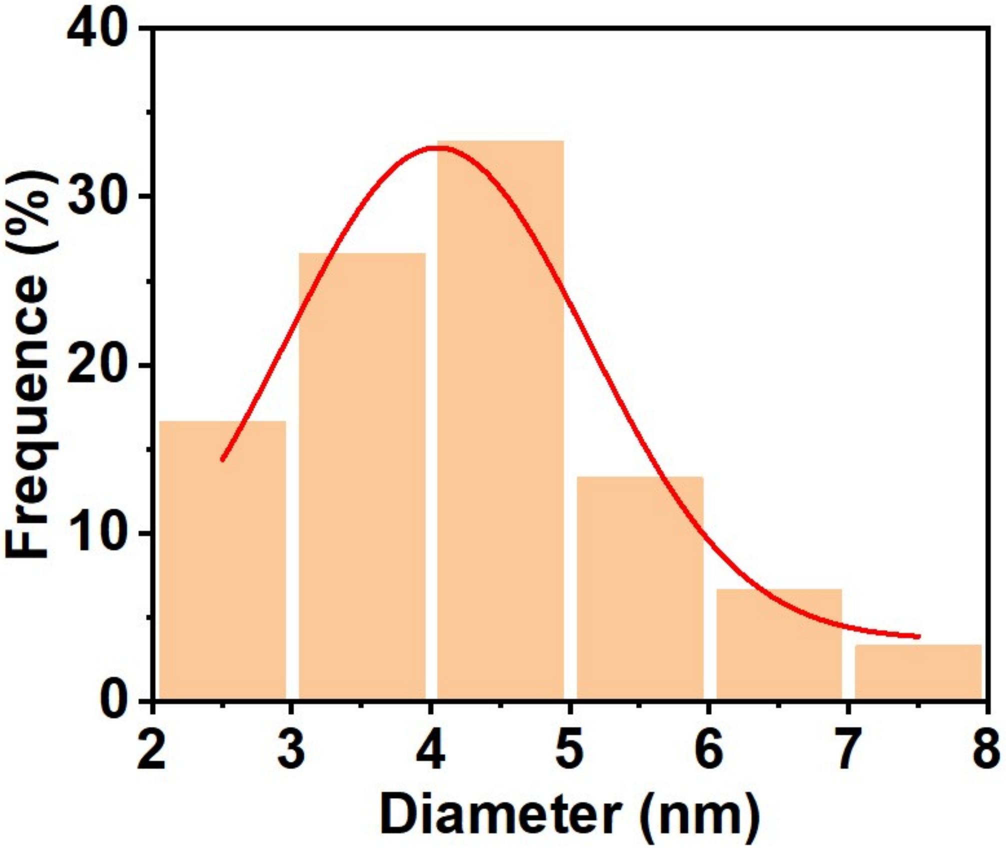

Figure S6. The particle size distribution diagram of HEA-15.

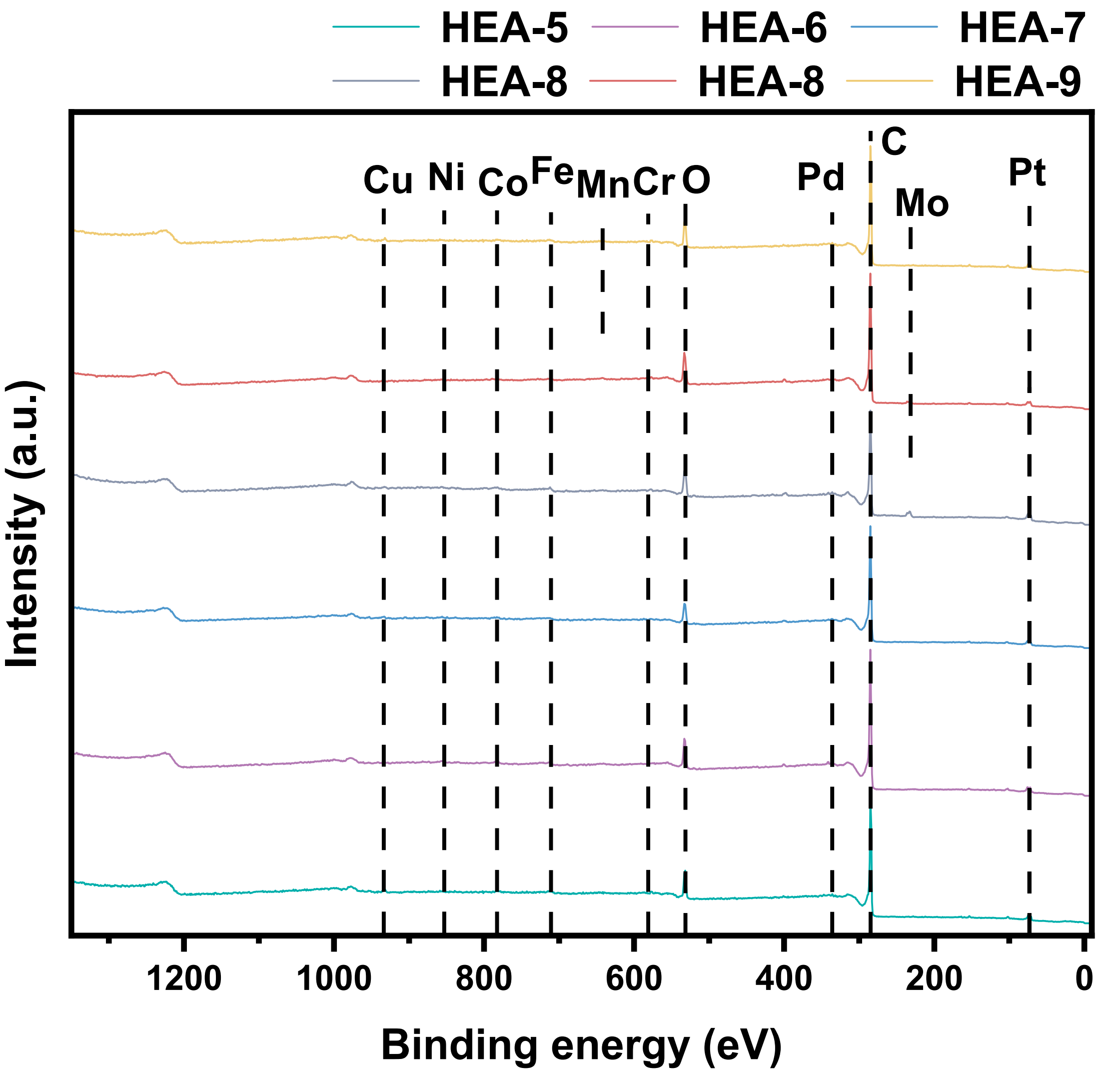

Figure S7. Survey XPS spectra of HEA-5, HEA-6, HEA-7, HEA-8 and HEA-9

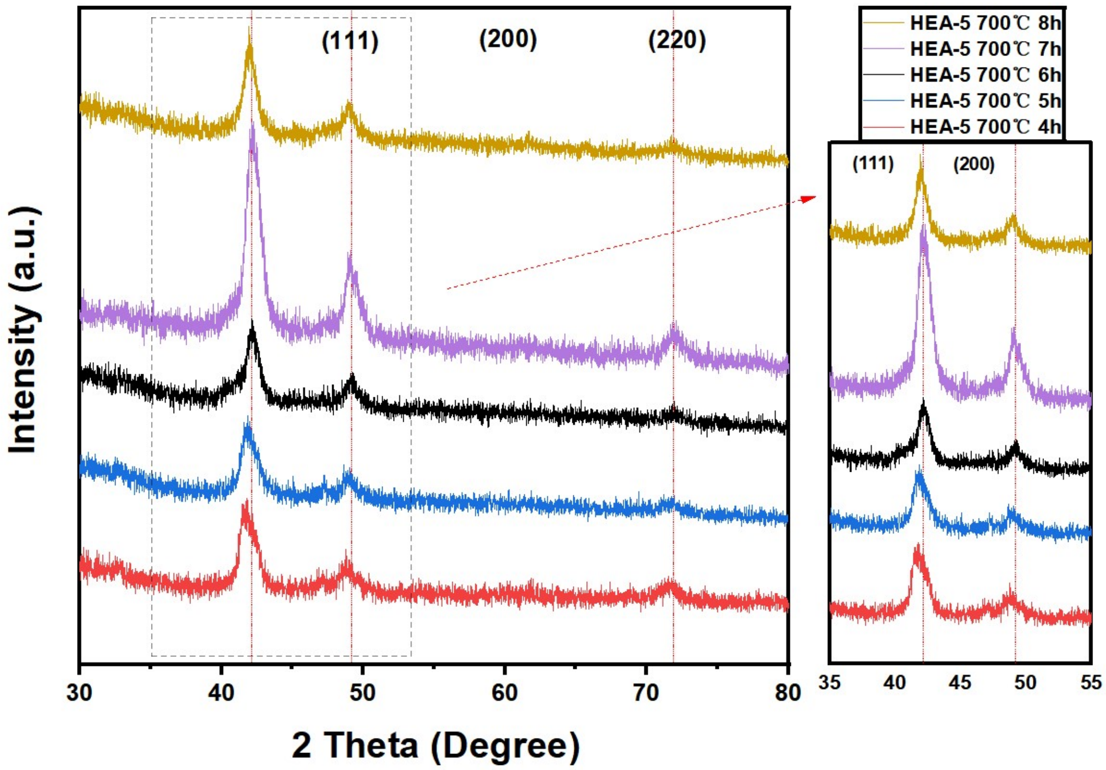

Figure S8. XRD of HEA-5 calcined at different holding times

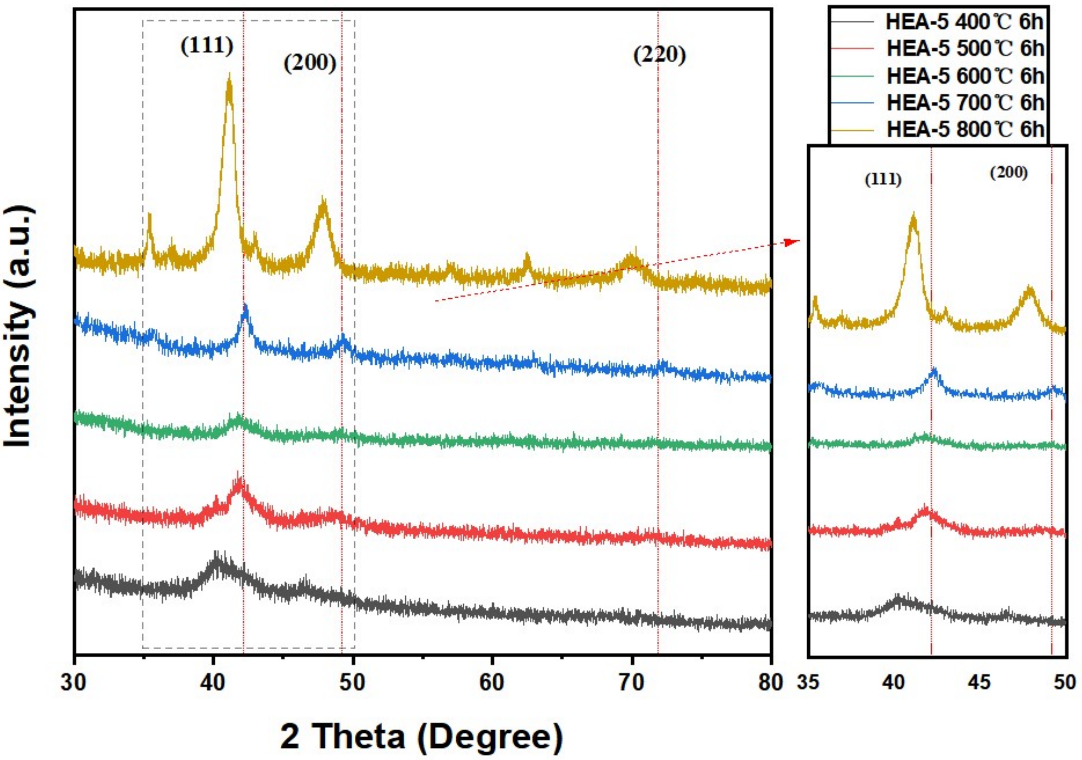

Figure S9. XRD of HEA-5 calcined at different temperatures

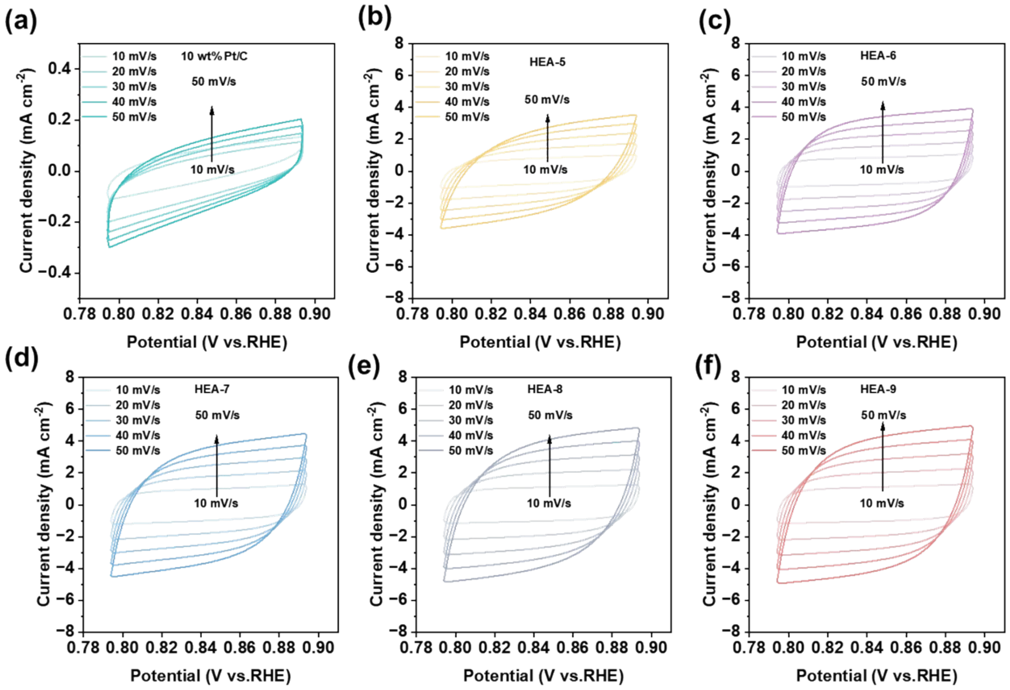

Figure S10. CV curves within a non-faradaic reaction region of -0.03 to -0.13 V (vs. RHE) at different scan rates toward HER for (a) 10 wt% Pt/C; (b) HEA-5; (c) HEA-6; (d) HEA-7; (e) HEA-8; (f) HEA-9.

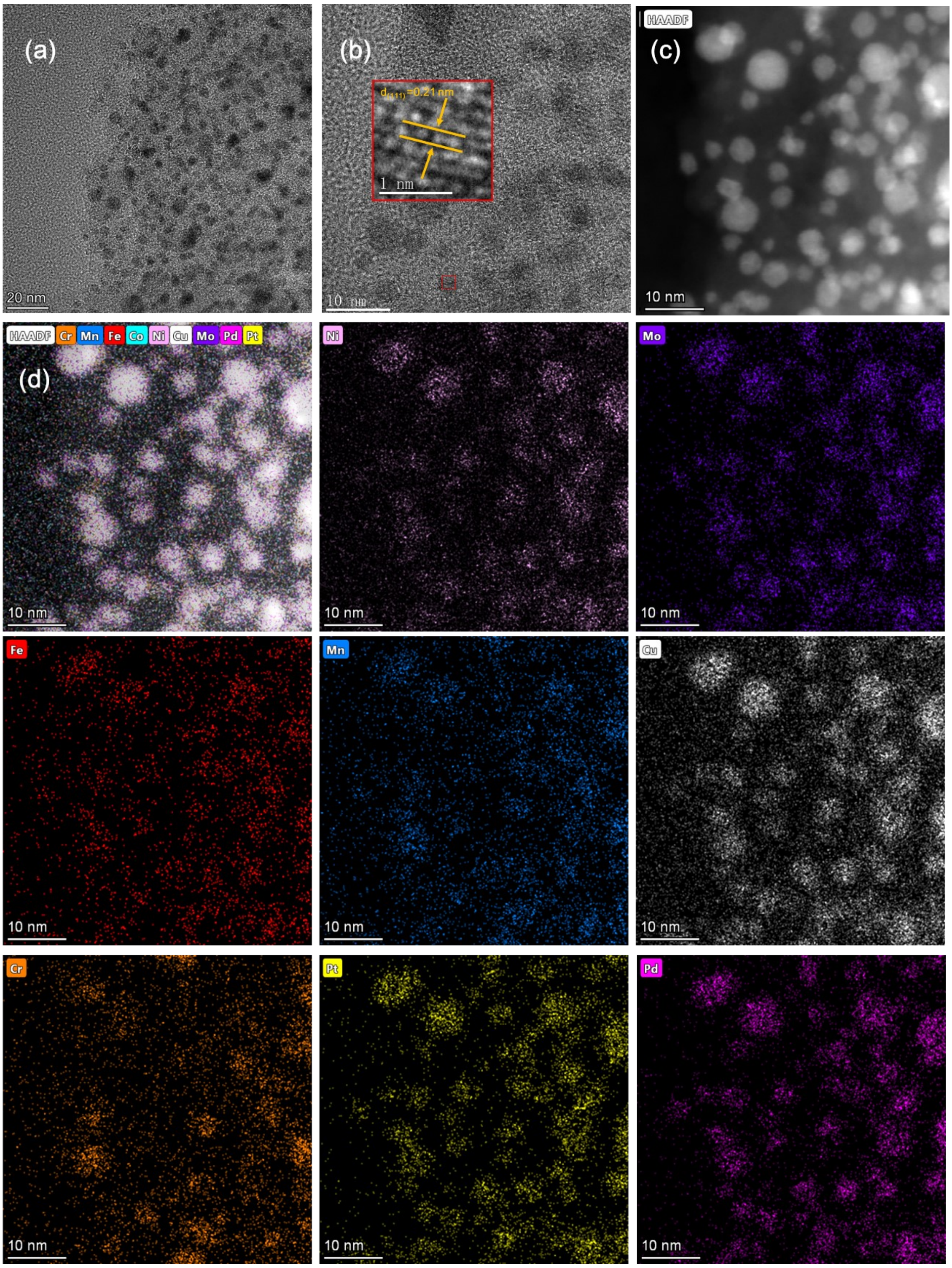

Figure S11. Post-stability structural characterization of HEA-9 after the HER durability test. (a-b) TEM images; (c) HAADF-STEM image; (d) corresponding EDS elemental mapping images of HEA-9 after the stability test.

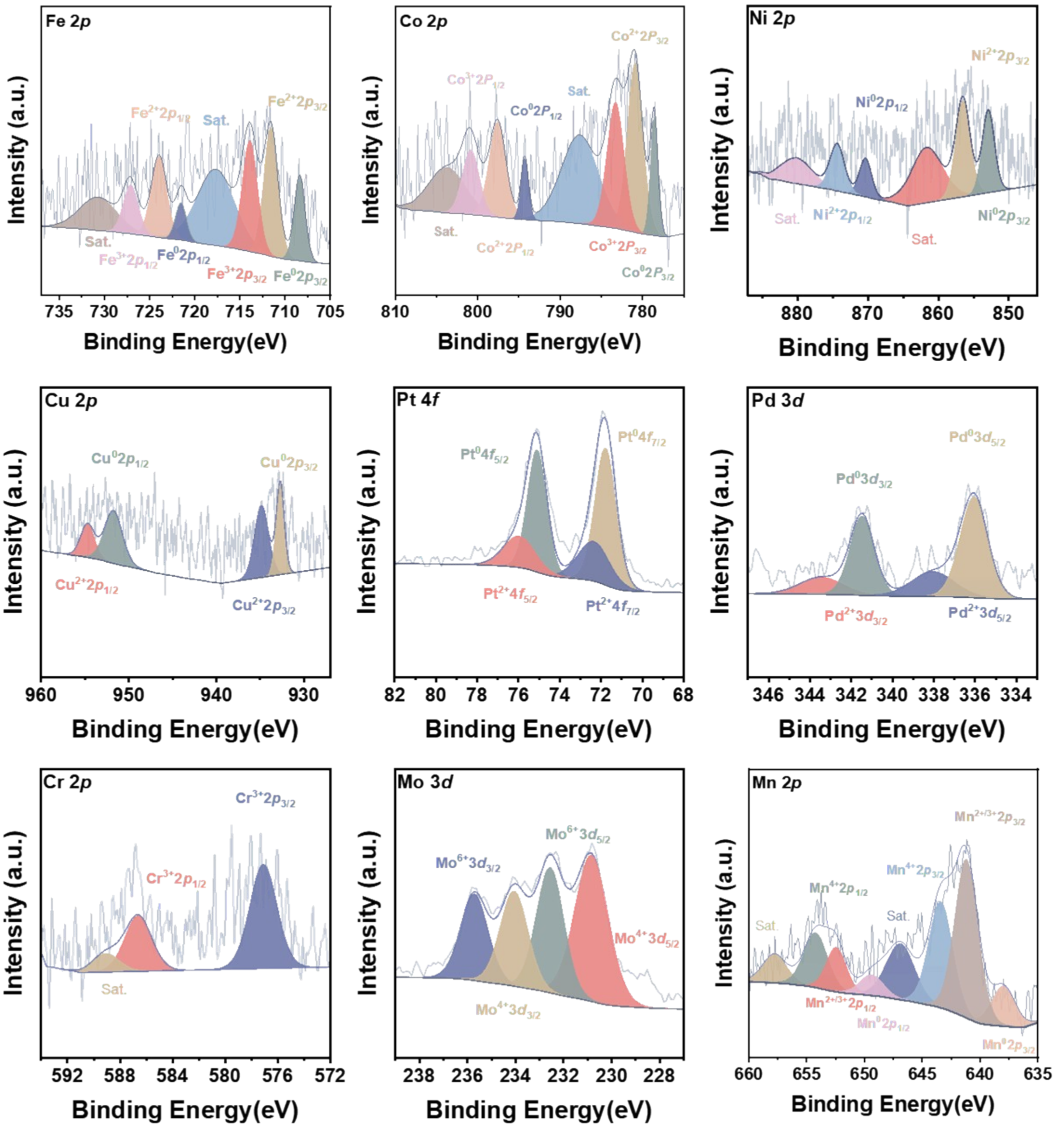

Figure S12. Post-stability XPS spectra of HEA-9 after the HER durability test, including Fe 2p, Co 2p, Ni 2p, Cu 2p, Pt 4f, Pd 3d, Cr 2p, Mo 3d, and Mn 2p core levels.

Fe	**0**								
Co	-1	0							
Ni	-2	0	0						
Cu	13	6	4	0					
Pt	-13	-7	-5	-12	0				
Pd	-4	-1	0	-14	2	0			
Cr	-1	-4	-7	12	-24	-15	0		
Mn	0	-5	-8	4	-28	-23	2	0	
Mo	-2	-5	-7	19	-28	-15	0	5	0
	Fe	Co	Ni	Cu	Pt	Pd	Cr	Mn	Mo

Table S1 | The mixing enthalpies of two elements (ΔH_{ij}^{mix})

Table S2 | The electronegativity and covalent radius of the involved metals.

Element	Electronegativity	Covalent Radius (pm)
Mn	1.55	139
Mo	2.16	145
Fe	1.83	125
Co	1.88	126
Ni	1.91	121
Cu	1.90	138
Pt	2.28	128
Pd	2.20	131
Cr	1.66	127

Note: An online tool was used: https://ptable.com/?lang=en#Properties/Series

Table S3 | The charge transfer resistance (R_{ct}) of different samples

Catalyst.	**R_{ct}(ohm)**
HEA-5	13.80
HEA-6	12.41
HEA-7	10.94
HEA-8	6.13
HEA-9	5.26
10 wt% Pt/C	14.93